Phys Chem Minerals
DOI 10.1007/s00269-006-0107-9

ORIGINAL PAPER

On the mechanisms for H and Al incorporation in stishovite

Geoffrey D. Bromiley · Fiona A. Bromiley · David W. Bromiley

Received: 20 February 2006 / Accepted: 15 August 2006

Abstract The solubility and incorporation mechanisms of hydrogen in synthetic stishovite as a function of Al_2O_3 content have been investigated. Mechanisms for H incorporation in stishovite are more complex than previously thought. Most H in stishovite is incorporated via the Smyth et al. (Am Mineral 80:454–456, 1995) model, where H docks close to one of the shared O–O edges, giving rise to an OH stretching band in infrared (IR) spectra at 3,111–3,117 cm^{-1}. However, careful examination of IR spectra from Al-stishovite reveals the presence of an additional OH band at 3,157–3,170 cm^{-1}. All H is present on one site, with interstitial H both coupled to Al^{3+} substitutional defects on adjacent octahedral (Si^{4+}) sites, and decoupled from other defects, giving rise to two distinct absorption bands. Trends in IR data as a function of composition are consistent with a change in Al incorporation mechanism in stishovite, with Al^{3+} substitution for Si^{4+} charge-balanced by oxygen vacancies at low bulk Al_2O_3 contents, and coupled substitution of Al^{3+} onto octahedral (Si^{4+}) and interstitial sites at high bulk Al_2O_3 contents. Trends in OH stretching frequencies as a function of Al_2O_3 content suggest that any such change in Al incorporation mechanism could alter the effect that Al incorporation has on the compressibility of stishovite, as noted by Ono et al. (Am Mineral 87:1486–1489, 2002).

G. D. Bromiley (✉)
Department of Earth Sciences, University of Cambridge, Downing Street, Cambridge CB2 3EQ, UK
e-mail: gbro04@esc.cam.ac.uk

G. D. Bromiley · F. A. Bromiley
Bayerisches Geoinstitut, Universität Bayreuth, Bayreuth, Germany

D. W. Bromiley
Department of Earth Sciences, University of Bristol, Bristol, UK

Introduction

Incorporation of hydrogen into nominally anhydrous, high-pressure phases provides a mechanism for transporting 'water' into the Earth's mantle during subduction of oceanic lithosphere. H incorporation also has a significant effect on a range of mineral properties from electrical conductivity to rheology. The high-pressure silica polymorph stishovite accounts for 10–20% by volume of material in basaltic compositions under conditions of the Earth's Transition Zone and Lower Mantle (Ono et al. 2001). Several studies (Chung and Kagi 2002; Panero et al. 2003; Pawley et al. 1993) have demonstrated that stishovite can contain significant amounts of H charge-balanced by substitution of Al^{3+} for Si^{4+}.

The exact location of H in stishovite is uncertain. Smyth et al. (1995) suggested that H could be incorporated at a (0.42, 0.5, 0) position, close to the shared O–O edge, similar to the location of H in rutile, as refined from neutron diffraction data by Swope et al. (1995). This H position is counter-intuitive, because it implies H docking close to the shortest O–O distance in the stishovite (and rutile) structure. In contrast, results of first-principles modelling (Gibbs et al. 2004) suggest that H is more stable at a (0.44, 0.12, 0.0)

position, with vibration of the OH dipole towards one of the vacant channels in the stishovite structure. In all previous investigations it has been assumed that interstitial H ($H_i^{\cdot}$) is coupled with Al substitutional defects on adjacent octahedral Si sites (Al'_{Si}) [using Kröger and Vink (1956) notation], forming a coupled defect. The exact mechanism for H incorporation in stishovite is important because it will influence both H solubility and the effects of H incorporation on mineral properties. Furthermore, mechanisms for H incorporation in stishovite are related to Al incorporation. It has been suggested (Ono et al. 2002) that incorporation of Al has a significant effect on compressibility of the stishovite structure, and by inference, could have an influence on slab buoyancy under conditions of the Earth's deep mantle. Here, we conduct a detailed spectroscopic investigation of H incorporation in stishovite as a function of Al_2O_3 content.

Experimental details

All samples were synthesized at 15 GPa, 1,500°C using a 1,200 tonne MA8 Kawai-type multi-anvil press, WC anvils and a 14M sample assembly at the Bayerisches Geoinstitut [see Demouchy et al. (2005) for further details]. Starting mixes of SiO_2 (99.995% purity) and $Al(OH)_3$ (99.99% purity) were loaded into welded Pt capsules (0.1 mm wall thickness, 1.6 mm outer diameter) with 5 wt% distilled water. Runs were fully pressurized and then heated at a rate of 100°C min^{-1}. Temperature was maintained for 4–5 h and runs quenched by switching off power to the heating circuit. After recovery, capsules were pierced, weighed and heated to check for the presence of water. Runs in which water was not present were discounted. Capsules were sectioned longitudinally, with one half prepared for electron microprobe analysis (EMPA) and the other half as a 30 μm thick doubly polished thin section or as individual, doubly polished, optically oriented crystal mounts. Phases were identified optically and by Raman spectroscopy, and water incorporation studied using Fourier transform infrared (IR) spectroscopy. Five hundred and twelve scans were obtained for each spectrum at a resolution of 1 cm^{-1}, using a Bruker IFS 120 HR high-resolution FTIR spectrometer coupled with a Bruker IR microscope containing all-reflecting Cassegranian optics. Measurements were taken using a tungsten light source, a silicon-coated CaF_2 beamsplitter and a narrow-band MCT detector. For polarized measurements a wire-strip polarizer on a KRS-5 substrate was used. The optics of the spectrometer were kept under vacuum, and the optics of the microscope were continually purged with CO_2 and H_2O-free, purified air to prevent the appearance of anomalous absorption bands. Variable apertures in the rear focal plane of the ×15 Cassegranian objective were used to obtain spectra from crack- and inclusion-free areas of crystals. For all measurements, samples were placed on thin CaF_2 plates and immersed in poly-trichlorofluoroethylene oil to prevent the occurrence of interference fringes [see Bromiley and Keppler (2004) for further details]. For some samples, hand-picked crystals were large enough to be prepared as oriented, polished thin sections and polarized IR spectra were obtained. For other samples, small crystal size meant that only unpolarized spectra could be obtained. To allow comparison of IR spectra and calculated water contents between all samples, water contents were calculated from total absorbencies over the entire OH stretching range using the calibration of Pawley et al. (1993). Libowitzky and Rossman (1996) note that determination of water contents based on unpolarized radiation (of unoriented crystals) may give misleading results because of absorption band anisotropy. In order to determine water contents accurately, spectra should be taken using polarized radiation parallel to the three main axes of the indicatrix. However, it was recently shown by Asimov et al. (2006) that in cases where oriented single-crystals cannot be prepared, statistical analysis of randomly oriented crystals can be used to determine water contents. This implies that if spectra can be obtained from a sufficient number of unoriented crystals, averaged water contents will eventually converge on a correct mean value. This approach can only work if spectra from a sufficiently large number of (randomly oriented) crystals can be obtained, and is also reliant upon the fact that all crystals have the same water content (i.e. representative of some equilibrium value). For determining water contents, we collected unpolarized spectra from between 28 and 49 crystals in each sample. Comparison of spectra from oriented crystals from the same sample demonstrated that water contents had reached equilibrium values (as would be expected given the long run times and rapid diffusion of H). Furthermore, good agreement was noted between measured absorbencies from polarized and averaged unpolarized spectra for several of the samples.

Compositions of stishovite samples were determined using a Cameca SX100 Electron Microprobe, with wave dispersive spectrometry at the Department of Earth Sciences, University of Bristol. A beam current of 10 nA and accelerating voltage of 20 keV was used, and Al and Si were analysed using albite and wollastonite standards, respectively. Over 40 point analyses were taken for each sample, and compositions averaged.

Table 1 Experimental details, phase identification and compositions

Run no.	Al_2O_3 content of starting mix (wt%)	Run products[a]	Composition[b]			Water content (ppm H_2O wt)[b]
			Al_2O_3	SiO_2	Total	
AlSt6	5	St + cor + f	3.15(6)	96.32(135)	99.47(138)	Not analysed
AlSt8	0	St + f	0	99.97(18)	99.97(18)	3 ± 1
AlSt9	0.5	St + f	0.59(12)	99.30(28)	99.89(46)	226 ± 96
AlSt12	1	St + f	1.09(26)	98.51(72)	99.60(63)	455 ± 193
AlSt11	2	St + f	1.94(31)	97.81(43)	99.75(30)	456 ± 194
AlSt10	3	St + f	2.95(15)	96.36(135)	99.31(59)	385 ± 163

Errors on the last significant figure are given in parentheses

[a] *st* stishovite, *cor* corundum, *f* fluid

[b] Quoted errors are absolute errors, derived from the error on the Pawley et al. (1993) calibration

Results

Details of run products and compositions are listed in Table 1. EMPA and polarized IR analysis show that Al_2O_3 and H_2O contents are homogeneous in samples studied, implying attainment of equilibrium. The presence of corundum in AlSt6 demonstrates that under the run conditions, maximum Al_2O_3 solubility in stishovite is 3.15 wt%. Subsequent experiments were performed using Al_2O_3 contents from 0 to 3.0 wt%. In all subsequent experiments, Al_2O_3 contents of stishovite samples were, within error, the same as bulk Al_2O_3 contents of the starting mixes. This is consistent with the absence of any additional phases in run products, as verified from detailed optical analysis and examination of back-scattered images of prepared samples during EMPA. Figure 1 shows polarized IR spectra obtained from nominally Al-free stishovite and Al-stishovite. Spectra from Al-free stishovite contain OH absorption bands at 3,311, 3,238 and 3,111 cm^{-1}. The OH band at 3,111 cm^{-1} is highly anisotropic, and has an approximately 95% component of vibration perpendicular to the crystallographic *c* axis. The absorption bands at 3,311 and 3,238 cm^{-1} have markedly different anisotropies, and clearly represent H incorporated on different sites. IR spectra from all Al-bearing stishovites differ significantly from Al-free stishovite and only contain one assymetrical OH absorption feature centred at 3,111–3,115 cm^{-1}. This absorption feature clearly comprises two OH absorption bands, a prominent band at 3,111–3,117 cm^{-1} (comparable to the OH band at 3,111 cm^{-1} in Al-free stishovite spectra), and an additional band at 3,158–3,167 cm^{-1} present as a shoulder on the main band. Both bands have a 95% component of vibration perpendicular to the crystallographic *c* axis.

Averaged unpolarized IR spectra from all samples are shown in Fig. 2. In order to determine trends in the position and areas of the OH absorption bands in Al-stishovite spectra, spectra were fitted using a full-profile Lorentzian fitting procedure. Peak fitting provides the only reliable method for determining how much 'water' is incorporated corresponding to the different OH absorption bands, because it is the area of these bands (the integrated absorbance) rather than the peak height that gives a measure of the amount of 'water' stored. Simple examination of changes in relative band height can give misleading results: this is especially the case for spectra shown in Fig. 2, because there are significant variations in both absorption band intensity and wavenumber as a function of composition, and these trends are different for the two main OH bands.

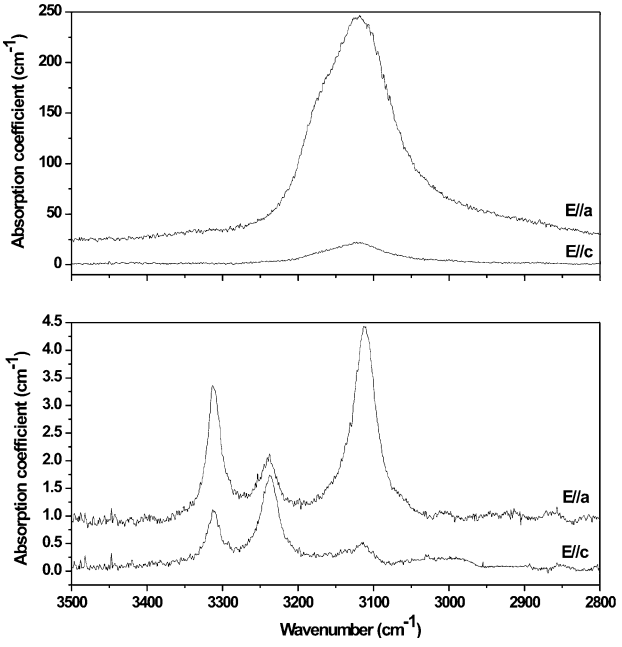

Fig. 1 Polarized NIR spectra from Al-free stishovite AlSt8 (*bottom*) and Al-bearing stishovite AlSt11 (*top*). Spectra offset vertically for clarity

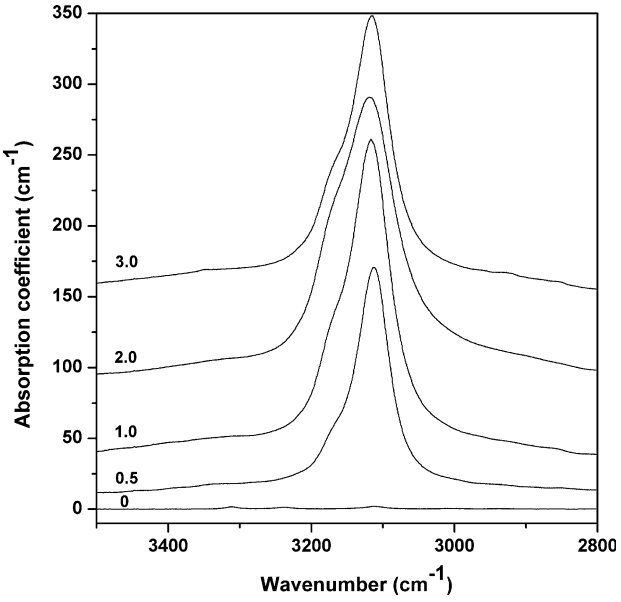

Fig. 2 Averaged (unpolarized) spectra from all stishovite samples, offset vertically with increasing Al_2O_3 content (*labelled*)

Data on band positions, widths and areas are listed in Table 2. Spectra were fitted over the region 4,000–2,500 cm^{-1} using two peaks corresponding to the main OH bands, and a broad background over the OH stretching region. For a meaningful fit of the data it was necessary to fix the full-width half-maximum of the IR band 2 at a constant value for all four (Al-stishovite) spectra. Using this procedure, we were able to provide excellent fits to the IR data. It should be noted that water contents (Table 1) were calculated from integrated absorbencies of averaged unpolarized spectra over the entire OH stretching region, as is specified by the calibration method of Pawley et al. (1993). It is not clear whether broad background absorption over the OH stretching region is due to structurally incorporated H or not. This feature was noted in spectra (both unpolarized and polarized) from all Al-bearing stishovites, and could not be removed by polishing. Likewise, spectra were only obtained from clear, crack- and inclusion-free areas of crystals. Mierdel and Keppler (2004) noted similar broad backgrounds over OH stretching regions in spectra obtained from $MgSiO_3$ enstatite synthesized at high pressure. Because the IR calibration method of Pawley et al. (1993) considers the area of this broad background feature in calculations of water contents, it is possible that this method leads to some overestimation of water contents and slight inconsistency with trends in integrated intensity of the main OH bands. Trends in the areas of the two OH bands (determined from the fit of IR data) and overall water contents as a function of Al_2O_3 content are shown in Fig. 3.

Discussion

Mechanisms for H incorporation in stishovite

Clear differences are seen between IR spectra from nominally Al-free and Al-bearing stishovite. These differences are also noted when comparing spectra presented by previous workers. Spectra from Al-free stishovite are similar to spectra obtained by Pawley et al. (1993), although there are slight differences in the relative intensities of the three absorption bands. Spectra from Al-bearing stishovite are similar to spectra by Chung and Kagi (2002) and Panero et al. (2003). The main mechanism for H incorporation in all samples is related to the presence of the absorption band at 3,111–3,117 cm^{-1}, which has a 95% component of vibration perpendicular to the crystallographic *c* axis. This is consistent with the H incorporation mechanism proposed by Smyth et al. (1995), where H is located close to one of the shared O–O edges. Gibbs et al. (2004) state that their model for H incorporation is more consistent with IR data from Chung and Kagi (2002), where vibration of the OH dipole is parallel to

Table 2 Areas and wavenumbers of the two main OH bands in Al-stishovite spectra determined by Lorentzian full-profile peak fitting

Run no.	Band 1			Band 2		
	Area (cm^{-2})	Position (cm^{-1})	Width[a] (cm^{-1})	Area (cm^{-2})	Position (cm^{-1})	Width[a,b] (cm^{-1})
AlSt9	36.5(3)	3,111.2(0)	49.70(12)	17.5(2)	3,156.7(3)	56.40
AlSt12	106.7(8)	3,115.0(0)	61.20(15)	13.3(1)	3,166.6(2)	56.40
AlSt11	265.7(38)	3,117.1(1)	84.93(38)	8.7(2)	3,170.0(3)	56.40
AlSt10	77.9(7)	3,114.0(1)	59.57(18)	22.0(2)	3,165.8(2)	56.40

Errors on the last significant figure are given in parentheses

[a] Full-width half-maximum

[b] Width of band 2 was fixed during Lorentzian fitting procedure

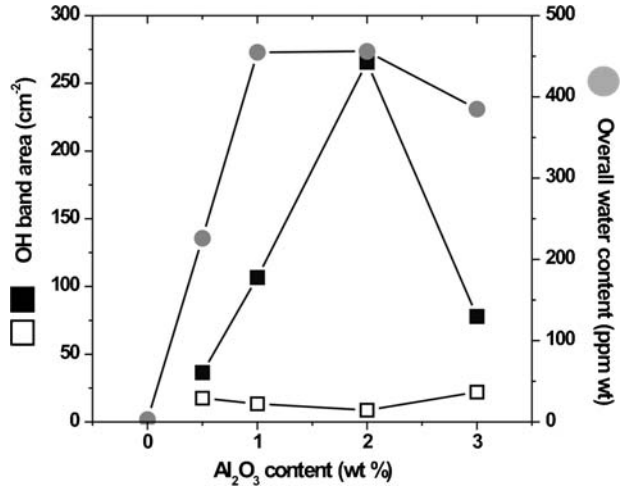

Fig. 3 Plot of area of OH stretching bands at 3,111–3,117 cm^{-1} (*filled square*) and 3,157–3,167 cm^{-1} (*open square*) and water content (*circle*) as a function of Al_2O_3 content of stishovite. Errors on absorption band areas are smaller than *symbols*. Absolute errors on calculated water contents are derived from the error on the Pawley et al. (1993) calibration (Table 1). Relative errors on calculated water contents are significantly smaller and are represented by the size of the *symbols*

the crystallographic *a* axis. However, Gibbs et al. (2004) actually report an OH bond angle of 93° for interstitial H coupled with Al substitution onto an adjacent Si octahedral site. This is for a ground state configuration, so allowing for the effects of thermal vibration on OH bond angles, and considering possible error in crystal alignment in the present IR data, it can be taken that IR data here are also consistent with the H incorporation model of Gibbs et al. (2004). An O–H stretching frequency of 3,111 cm^{-1} implies moderate to strong H bonding (Libowitzky 1999), again in accordance with both models. Al^{3+} incorporation in stishovite (i.e. substitution for Si^{4+}) has been assumed to provide the main mechanism for charge-balancing H incorporation, resulting in the formation of coupled Al'_{Si}–$H_i^{\cdot}$ defects, giving rise to the 3,111–3,117 cm^{-1} absorption band. However, this band is noted in spectra from nominally Al-free stishovite (sample AlSt8). The amount of water present in this sample is small, and the area of the 3,111 cm^{-1} band in the AlSt8 spectra corresponds to just over 1 ppm H_2O. Analysis of the SiO_2 used in this study (data from Alfa-Aesar) reveals that a trace amount of Al (8.2 ppm) is present. If we assume that all of this Al charge-balances H incorporation, then the amount of Al present would correspond to about 0.7 ppm H_2O. Given inherent inaccuracies in the calibration of water content in stishovite, this amount of Al is sufficient to explain H incorporation via the formation of coupled Al'_{Si}–$H_i^{\cdot}$ defects.

The additional OH band in all Al-stishovite spectra at 3,157–3,170 cm^{-1} is more problematic. This band exhibits exactly the same anisotropy as the band at 3,111–3,117 cm^{-1}, with a 95% component of vibration perpendicular to the crystallographic *c* axis. The presence of two distinct IR bands could be explained by H incorporation via both the Smyth et al. (1995) and Gibbs et al. (2004) models. However, given the inherent differences between these two models, this appears unlikely. An alternative assignment of OH absorption bands in stishovite can be presented if we reassess the assumption that Al'_{Si} and $H_i^{\cdot}$ defects in stishovite are coupled. Smyth et al. (1995) based their model of H incorporation in stishovite on the results of an investigation of H incorporation in rutile (Swope et al. 1995), which is isostructural with stishovite. Swope et al. (1995) refined the H position in a natural, H-rich rutile crystal from single-crystal neutron data, and demonstrated that H is located close to the shared O–O edge. IR spectra from natural and synthetic rutile often contain a number of distinct OH absorption bands despite the fact that only one H position can be refined from neutron data (Vlassopoulos et al. 1993). Bromiley and Hilairet (2005) recently reinvestigated mechanisms for H incorporation in rutile and found evidence for coupling of interstitial H with substitution of various trivalent and divalent cations for Ti^{4+} (i.e. formation of coupled defects directly analogous to the formation of Al'_{Si}–$H_i^{\cdot}$ defects in stishovite). However, Bromiley and Hilairet (2005) also suggested that 'decoupled' $H_i^{\cdot}$ defects could be present in rutile, namely, $H_i^{\cdot}$ not coupled to substitutional impurities on adjacent octahedral sites. Subsequent investigation of the effects of neutron irradiation and post-irradiation annealing on H incorporation in synthetic rutile (Bromiley and Shiryaev 2006) demonstrate that this is, indeed, the case. In synthetic rutile, this decoupled $H_i^{\cdot}$ gives rise to an additional absorption band at 3,279 cm^{-1}. Bromiley and Hilairet (2005) demonstrated that coupling of $H_i^{\cdot}$ with different substitutional impurities in rutile results in a shift in OH stretching frequencies due to Next-Nearest-Neighbour (NNN) effects. By analogy with rutile, we can, therefore, offer an alternative assignation of the 3,111–3,117-cm^{-1} OH band in stishovite spectra, where this band is due to isolated $H_i^{\cdot}$ defects not coupled to Al'_{Si}. This then allows a reinterpretation of mechanisms for H incorporation in stishovite. The presence of H in nominally Al-free stishovite, in particular the band at 3,111 cm^{-1}, no longer requires the presence of trace amounts of Al as an impurity. In Al-stishovite, the additional band at 3,157–3,170 cm^{-1} can then be assigned to $H_i^{\cdot}$ that becomes coupled to Al'_{Si} (that is, forming the Al'_{Si}–$H_i^{\cdot}$ defect cluster). If

correct, this implies that H is incorporated in stishovite via the Smyth et al. (1995) model. The H position proposed by Gibbs et al. (2004) is only consistent with IR data on O–H bond vibration if $H_i^{\cdot}$ is coupled with $Al_{Si}^{/}$. For uncoupled $H_i^{\cdot}$, Gibbs et al. (2004) calculated a corresponding O–H bond distance of 1.69 Å, which is too long to account for O–H stretching in stishovite IR spectra. In contrast, they calculated an O–H bond distance of 1.02 Å for $H_i^{\cdot}$ coupled to $Al_{Si}^{/}$, which is consistent with IR data, implying that the Gibbs et al. (2004) model of H incorporation in stishovite in an interchannel site cannot be used to assign IR bands that are split due to NNN effects.

Using current experimental data, it is not possible to conclusively demonstrate which of the two models for H incorporation in stishovite is correct. The main difference between the two models relates to the interaction of $Al_{Si}^{/}$ and $H_i^{\cdot}$ in stishovite. In both models, Al substitution provides the main charge-balancing mechanism for H incorporation. In the first model, H incorporation is charge-balanced locally, while in the second model, decoupling of defects implies that charge is balanced over the whole of the stishovite lattice.

The presence of small, additional OH bands in nominally Al-free stishovite spectra is problematic, because there are not sufficient quantities of lower valence cations present in the samples to charge-balance additional H incorporation. Alternatively, H incorporation in nominally pure SiO_2 stishovite could be charge-balanced by a very low concentration of Si^{4+} vacancies. Clearly, the absorption bands at 3,311 and 3,238 cm^{-1} have markedly different anisotropies than the main OH band at 3,111–3,117 cm^{-1}, implying very different mechanisms for H incorporation. In addition, the higher wavenumbers of these two bands imply weaker H bond interactions than the main band at 3,111–3,117 cm^{-1}. It is conceivable that these bands could relate to interstitial H associated with octahedral vacancies. This would be analogous to H incorporation in omphacite, which Smyth et al. (1991) suggested was related to the presence of M2 vacancies. Gibbs et al. (2004) noted that H incorporation in stishovite associated with octahedral vacancies would be favourable, and could give rise to OH vectors directed along [1 1 0] and [2 2 5]. The absence of these higher wavenumber bands in spectra from Al-rich stishovite samples could imply that the incorporation mechanism(s) that give rise to these additional absorption bands are inherently less stable, and can only operate in systems with very low Al contents.

Mechanisms for Al incorporation in stishovite

From Table 1 it can be seen that the concentration of Al in all samples (except AlSt8) is much higher (4–8 times) than H concentration. Therefore, the concentration of H in the samples is not sufficient to satisfy the electro-neutrality condition where substitution of Al^{3+} for Si^{4+} is charge-balanced by incorporation of H^{+}. Alternatively, Al^{3+} incorporation in stishovite must be charge-balanced by one of two mechanisms (Hirose et al. 2005). Firstly, Al^{3+} can substitute for Si^{4+}, charge-balanced by oxygen vacancies:

$$2Si_{Si}^{x} + O_{O}^{x} + Al_2O_3 \rightarrow 2Al_{Si}^{/} + V_{O}^{\cdot\cdot} + 2(SiO_2) \quad (1)$$

Secondly, Al^{3+} substitution for octahedral Si^{4+} can be charge-balanced by coupled substitution of Al^{3+} onto the large, distorted octahedral, interstitial sites in the stishovite structure:

$$3Si_{Si}^{x} + 2(Al_2O_3) \rightarrow 3Al_{Si}^{/} + Al_i^{\cdot\cdot\cdot} + 3(SiO_2) \quad (2)$$

Previous authors (Chung and Kagi 2002; Panero et al. 2003; Pawley et al. 1993) note that Al is probably incorporated in stishovite via mechanism [1]. Direct evidence for Al substitution for Si was found by Smyth et al. (1995) on the basis of refinement of single-crystal X-ray data from Al-bearing stishovite. Absence of evidence for interstitial Al by Smyth et al. (1995) is consistent with operation of mechanism [1]. Direct and indirect evidence from investigations of minor element incorporation in rutile (Bromiley and Hilairet 2005; Bromiley et al. 2004) has also demonstrated that the main mechanism for incorporation of lower valency cations in rutile involves substitution onto the octahedral (in this case Ti^{4+}) site, charge-balanced by oxygen vacancies. Mössbauer data obtained from Fe^{3+}-bearing rutile (Bromiley et al. 2004) demonstrate that Fe^{3+} is present on a relatively undistorted octahedral site. This is consistent with Fe^{3+} substitution for Ti^{4+}, but implies that if Fe-incorporation in rutile is charge-balanced by oxygen vacancies, the two cannot form a defect cluster (that is, $Fe_{Ti}^{/}$ and $V_{O}^{\cdot\cdot}$ defects are decoupled).

Investigations of rutile do, however, support the existence of cations on distorted interstitial sites in the structure under certain circumstances. The most notable example of this is the presence of interstitial Ti^{3+} in reduced, non-stoichiometric (TiO_{2-x}) rutile. Detailed spectroscopic examination of reduced rutile (Khomenko et al. 1998) demonstrates that electron sharing between Ti on adjacent interstitial and octahedral sites in rutile (i.e. $Ti^{3+}Ti^{4+}$ intervalence charge-transfer)

gives rise to the broad optical absorption that gives reduced rutile its characteristic intense blue colour.

Trends in H and Al solubility in stishovite

Regardless of the location of interstitial H in stishovite, the main mechanism for charge-balancing H incorporation is Al substitution for Si. However, as seen in Fig. 3, there is not a simple linear relationship between H solubility and Al content in stishovite. Instead, H solubility reaches a maximum around 1–2 wt% Al_2O_3 and then decreases. Trends in H solubility can be interpreted based on mechanisms for Al incorporation. As noted above, the main mechanism for Al incorporation in stishovite involves charge-balancing via oxygen vacancies. With increasing Al content, the increase in concentration of $V_O^{\cdot\cdot}$ could result in a decrease in H solubility. However, several other interesting trends in spectroscopic data are noted as a function of increasing Al content which cast doubt on this simple interpretation.

Fitting of IR data (Table 2) demonstrates that the positions of both OH bands in Al-stishovite spectra vary as a function of increasing Al content. For band 1 (3,111–3,117 cm^{-1}), the shift is fairly small. However, the shift in wavenumber for the smaller band 2 (3,157–3,170 cm^{-1}) is significantly greater. Smyth et al. (1995) noted an increase in octahedral volume in stishovite as a function of increasing Al content. Subsequent increases in O–O distances would, therefore, produce shifts in O–H stretching frequencies to higher values. However, although wavenumbers of the two OH bands increase with increasing Al_2O_3 content up to 2 wt%, there is a corresponding decrease in OH stretching frequencies between 2 and 3 wt% Al_2O_3. This appears to be inconsistent with Al incorporation charge-balanced solely by $V_O^{\cdot\cdot}$. Instead, these shifts provide evidence for additional substitution of Al^{3+} onto interstitial sites in stishovite at high Al contents (i.e. operation of mechanism [2]). This interpretation is supported by recent studies of rutile. Gesenhues and Rentschler (1999) investigated Al incorporation in rutile using X-ray and spectroscopic techniques and found that whilst Al substitution for Ti^{4+} was charge-balanced by oxygen vacancies at lower bulk Al_2O_3 contents, there was evidence for additional Al incorporation onto interstitial sites in the rutile structure at high bulk Al_3O_3 contents. The presence of $Al_i^{\cdot\cdot\cdot}$ defects in stishovite would signify a change in the dominant mechanism for Al incorporation, and would be expected to have a markedly different effect of octahedral volumes and O–O distances compared to Al–Si substitution charge-balanced by oxygen vacancies. This explains the change in the trend of O–H stretching frequencies noted in Table 2. The presence of interstitial Al would also result in a decrease in H solubility which would augment the effect of an increase in the concentration of oxygen vacancies. Alternatively, decrease in H solubility at high bulk Al_2O_3 contents could be due to a decrease in O–O distances.

Other interesting trends in the data are seen in the relative areas of the two OH absorption bands as a function of Al_2O_3 content. Changes in the area of band 1 reflect changes in the overall water content, because this band represents most of the OH incorporated in stishovite. However, changes in the area of band 2 are different. There is a decrease in band area up to 2 wt% Al_2O_3 followed by a slight increase. Decrease in the area of band 2 implies that the H incorporation mechanism giving rise to this band becomes less favourable with increasing Al_2O_3 content. This could represent some external crystallographic constraint (such as octahedral volume and O–O distances) on the stability of interchannel H vs H incorporated via the Smyth et al. (1995) mechanism, or the proportion of coupled vs decoupled H, depending upon which assignment of OH bands is correct. A subsequent increase in the area of OH band 2 at higher bulk Al_2O_3 contents is then consistent with a change in Al incorporation mechanism. However, for interchannel H, the presence of interstitials (i.e. interchannel Al) would be expected to offset this trend, and result in a decrease in H affinity. This is not the case if band 2 is assigned to coupled $H_i^{\cdot}$–$Al_{Si}^{\prime}$ defects incorporated via the Smyth et al. (1995) mechanism, because we would anticipate some additional increase in the area of band 2 OH with increasing Al_2O_3 content anyway, because of a simple statistical effect (i.e. an increase in the probability of coupling of randomly interacting defects).

Summary and implications for the role of stishovite

In Al-bearing stishovite, there appear to be two mechanisms for H incorporation. In the first model, H is coupled to Al substitution for Si. The presence of two OH bands is due to H incorporation via both the Smyth et al. (1995) and Gibbs et al. (2004) models. In the second model, all H is incorporated via the same mechanism, and the difference in O–H stretching frequencies is assigned to a NNN effect. That is, the band at 3,111–3,117 cm^{-1} is assigned to H decoupled from Al defects, with the additional band shifted to 3,157–3,170 due to H docking adjacent to an AlO_6 octahedron. In this case, H must be incorporated via the Smyth et al. (1995) model, because Gibbs et al. (2004) note that there model is only consistent with IR data if $H_i^{\cdot}$ is

coupled with Al'_{Si} defects. Although experimental data cannot conclusively demonstrate which of these two models is correct, several observations support the latter interpretation:

1. Anisotropies of both OH bands are identical and O–H stretching frequencies very close to each other.
2. The shift in O–H stretching frequency of band 2 relative to band 1 is of the correct magnitude, and in the correct direction that would be predicted based on the effect of Al–Si substitution on O–O distances using the X-ray data of Smyth et al. (1995) and the calibration of O–O distance vs O–H stretching frequency of Libowitzky (1999).
3. H incorporation in stishovite appears to be similar to H incorporation in rutile, to which it is isostructural. Both coupled and decoupled $H^{\cdot}_i$ defects are present in synthetic rutile (Bromiley and Hilairet 2005; Bromiley and Shiryaev 2006).
4. The presence of the 3,111–3,117-cm^{-1} band in nominally Al-free stishovite can only be assigned to coupled Al'_{Si}–$H^{\cdot}_i$ defects if all trace Al in the starting mix is used to charge-balance H incorporation, and H_2O contents reported in Table 1 are overestimated. In all other samples, concentration of Al is 4–8 times higher than H. The dominant mechanism for Al incorporation in stishovite appears to be Al–Si substitution charge-balanced by oxygen vacancies rather than H incorporation. If all Al incorporation in the nominally Al-free stishovite is charge-balanced by H incorporation this implies a major change in the relative stabilities of different defects in Al-poor vs Al-rich stishovite.

H solubility in stishovite depends on Al content, and on the mechanism for Al incorporation. H solubility reaches a maximum at 1–2 wt% Al_2O_3. The ability of stishovite to transport water in subducting slabs will depend on Al_2O_3 content, and by inference, on slab geochemistry. X-ray and spectroscopic data on minor element incorporation in stishovite is consistent with Al substitution for Si in stishovite charge-balanced by oxygen vacancies. However, at high bulk Al_2O_3 contents, Al may also substitute onto the large interstitial sites present in the stishovite structure. It has been shown that Al-substitution has a marked effect on stishovite compressibility (Ono et al. 2002), resulting in a decreased bulk modulus and increased density. Determination of the density of stishovite is of vital importance in understanding the fate of subducting slabs in the lower mantle because it affects slab buoyancy. However, work on the compressibility of Al-stishovite was conducting using samples containing 2.1 wt% Al_2O_3, so interstitial Al was probably not present. The effect of higher Al_2O_3 contents on OH band positions (Table 2) implies that the presence of interstitial Al could result in a subsequent decrease in cell parameters, and presumably, some additional effect on compressibility. Data from phase stability studies on phase egg (Ono 1999) suggest that Al_2O_3 solubility in stishovite varies significantly as a function of pressure and temperature, so changes to the compressibility of stishovite could be complex. Mechanisms for, and solubility of Al in stishovite will also have a major impact on H solubility, and could constrain the effectiveness of stishovite in terms of water transport into the transition zone and lower mantle.

Acknowledgments GDB thanks Dan Frost for help with MA experiments and Hans Keppler for providing additional access to IR facilities at the BGI. This manuscript was improved following comments by David F. Cox and an anonymous reviewer.

References

Asimov P, Stein L, Mosenfelder J, Rossman G (2006) Quantitative polarized infrared analysis of trace OH in populations of randomly oriented mineral grains. Am Mineral 86:147–158

Bromiley GD, Hilairet N (2005) An investigation of hydrogen and minor element incorporation in synthetic rutile. Mineral Mag 69(3):345–358

Bromiley GD, Keppler H (2004) An experimental investigation of hydroxyl solubility in jadeite and Na-rich pyroxenes. Contrib Mineral Petrol 147:189–200

Bromiley GD, Shiryaev AA (2006) Neutron irradiation and post-irradiation annealing of rutile (TiO_{2-x}): effect on hydrogen incorporation and optical absorption. Phys Chem Miner 33:426–434

Bromiley GD, Hilairet N, McCammon C (2004) Solubility of hydrogen and ferric iron in rutile and TiO_2 (II): implications for phase assemblages during ultrahigh-pressure metamorphism and for the stability of silica polymorphs in the lower mantle. Geophys Res Lett 31:L04610

Chung J, Kagi H (2002) High concentration of water in stishovite in the MORB system. Geophys Res Lett 29(21). DOI 10.1029/2002GL015579

Demouchy S, Deloule E, Frost D, Keppler H (2005) Pressure and temperature-dependence of water solubility in Fe-free wadsleyite. Am Mineral 90:1084–1091

Gesenhues U, Rentschler T (1999) Crystal growth and defect structure of Al^{3+}-doped rutile. J Solid State Chem 143:210–218

Gibbs G, Cox D, Ross N (2004) A modeling of the structure and favourable H-docking sites and defects for the high-pressure silica polymorph stishovite. Phys Chem Miner 31:232–239

Hirose K, Takafuji N, Sata N, Ohishi Y (2005) Phase transition and density of subducted MORB crust in the lower mantle. Earth Planet Sci Lett 23(1–2):239–251

Khomenko V, Langer K, Rager H, Fett A (1998) Electronic absorption by Ti^{3+} ions and electronic delocalization in synthetic blue rutile. Phys Chem Miner 25:338–346

Kröger FA, Vink HJ (1956) Relations between the concentrations of imperfections in crystalline solids. In: Seitz F,

Turnball D (eds) Solid state physics: advances and applications, vol 3. Academic, New York, pp. 307–435
Libowitzky E (1999) Correlation of O–H stretching frequencies and O–H···O hydrogen bond lengths in minerals. Monatsh Chem 130(8):1047–1059
Libowitzky E, Rossman G (1996) Principles of quantitative absorbance measurements in anisotropic crystals. Phys Chem Miner 23:319–327
Mierdel K, Keppler H (2004) The temperature dependence of water solubility in enstatite. Contrib Mineral Petrol 148(3):305–311
Ono S (1999) High temperature stability limit of phase egg, $AlSiO_3(OH)$. Contrib Mineral Petrol 137:83–89
Ono S, Ito E, Katsura T (2001) Mineralogy of subducted basaltic crust (MORB) from 25 to 37 GPa, and chemical heterogeneity of the lower mantle. Earth Planet Sci Lett 190:57–63
Ono S, Suto T, Hirose K, Kuwayama Y, Komabayashi T, Kikegawa T (2002) Equation of state of Al-bearing stishovite to 40 GPa at 300 K. Am Mineral 87(10):1486–1489
Panero W, Benedetti L, Jeanloz R (2003) Transport of water into the lower mantle: role of stishovite. J Geophy Res 108(B1). DOI 10.1029/2002JB002053
Pawley A, McMillan P, Holloway J (1993) Hydrogen in stishovite, with implications for mantle water-content. Science 261(5124):1024–1026
Smyth J, Bell D, Rossman G (1991) Incorporation of hydroxyl in upper-mantle clinopyroxenes. Nature 351:732–735
Smyth J, Swope R, Pawley A (1995) H in rutile-type compounds: II. Crystal chemistry of Al substitution in H-bearing stishovite. Am Mineral 80:454–456
Swope R, Smyth J, Larson A (1995) H in rutile compounds: I. Single-crystal neutron and X-ray diffraction study of H in rutile. Am Mineral 80:448–453
Vlassopoulos D, Rossman G, Haggerty S (1993) Coupled substitution of H and minor elements in rutile and the implications of high OH contents in Nb- and Cr-rich rutile from the upper mantl. Am Mineral 78:1181–1191